

Accepted Manuscript

Solid solution and amorphous phase in Ti-Nb-Ta-Mn systems synthesized by mechanical alloying

C. Aguilar, P. Guzman, S. Lascano, C. Parra, L. Bejar, A. Medina, D. Guzman



PII: S0925-8388(15)31964-2

DOI: [10.1016/j.jallcom.2015.12.173](https://doi.org/10.1016/j.jallcom.2015.12.173)

Reference: JALCOM 36262

To appear in: *Journal of Alloys and Compounds*

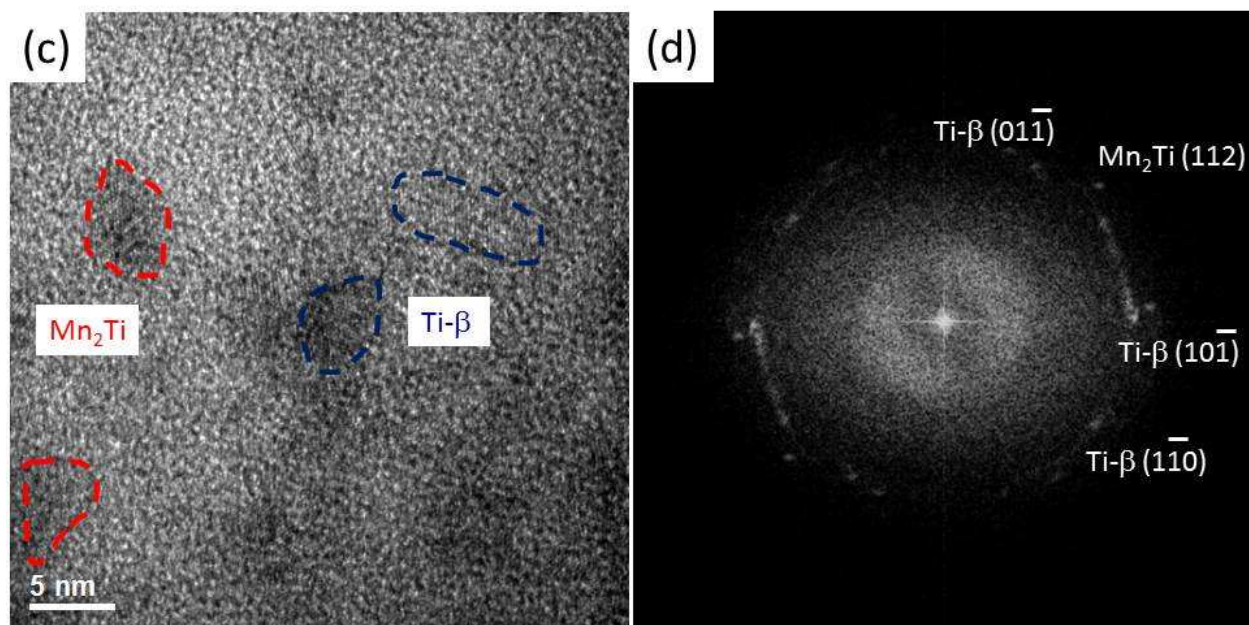
Received Date: 22 September 2015

Revised Date: 8 December 2015

Accepted Date: 21 December 2015

Please cite this article as: C. Aguilar, P. Guzman, S. Lascano, C. Parra, L. Bejar, A. Medina, D. Guzman, Solid solution and amorphous phase in Ti-Nb-Ta-Mn systems synthesized by mechanical alloying, *Journal of Alloys and Compounds* (2016), doi: 10.1016/j.jallcom.2015.12.173.

This is a PDF file of an unedited manuscript that has been accepted for publication. As a service to our customers we are providing this early version of the manuscript. The manuscript will undergo copyediting, typesetting, and review of the resulting proof before it is published in its final form. Please note that during the production process errors may be discovered which could affect the content, and all legal disclaimers that apply to the journal pertain.



ACCEPTED TEL

Solid solution and amorphous phase in Ti-Nb-Ta-Mn systems synthesized by mechanical alloying

C. Aguilar^{1a,*}, P. Guzman¹, S. Lascano^{1b}, C. Parra^{1c}, L. Bejar^{2c}, A. Medina^{2d}, D. Guzman³

(1) Departamento de Ingeniería Metalúrgica y Materiales^a, Departamento de Ingeniería Mecánica^b,
Departamento de Física^c, Universidad Técnica Federico Santa María, Av. España 1680, Valparaíso, Chile

(2) Instituto de Investigaciones Metalúrgicas^c, Facultad de Ingeniería Mecánica^d, Universidad Michoacana de
San Nicolás de Hidalgo, Ciudad Universitaria, Morelia, Michoacán, México. C.P. 58000

(3) Departamento de Metalurgia, Universidad de Atacama, Av. España 485, Copiapó, Chile.

(*) corresponding author: claudio.aguilar@usm.cl, phone/fax: 56-32-2654228

Abstract

This work discusses the formation of Ti-30Nb-13Ta-xMn (x: 2, 4 and 6 wt%) solid solution by mechanical alloying using a shaker mill. A solid solution was formed after 15 h of milling and an amorphous phase was formed after 30h of milling, according to X-ray diffraction results. Disappearance of strongest X-ray diffraction peaks of Nb, Ta and Mn indicated the formation of solid solution, while, X-ray diffraction patterns of powders milled for 30 h showed an amorphous hump with crystalline peaks in the angular range of 35 to 45° in 2θ. TEM image analysis showed the presence of nanocrystalline intermetallic compounds embedded in an amorphous matrix. Mn₂Ti, MnTi and NbTi₄ intermetallic compounds were detected and revealed crystallites with size ranging from 3 to 20 nm. The Gibbs free energy for the formation of solid solution and amorphous phase of three ternary systems (Ti-Nb-Ta, Ti-Nb-Mn and Ti-Ta-Mn) was calculated using extended Miedema's model. Experimental and thermodynamic data confirmed that solid solution was first formed in the alloy with 6wt% Mn followed by the formation of an amorphous phase as milling time increases. The presence of Mn promoted the formation of amorphous phase because the atomic radius difference between Mn with Ti, Nb and Ta.

Keywords: Metals and alloys, mechanical alloying, thermodynamic properties, X-ray diffraction, transmission electron microscopy, TEM

1 Introduction

Increased life expectancy of human beings is causing degenerative diseases such as the ones associated to degradation of the mechanical properties of the bone. It is estimated that 90% of the population (over 40-year old) suffer from these diseases [1]. Artificial biomaterials are one of the proposed solution for these problems as they expected to serve as implants or to replace bones. In this sense, metallic materials are already widely used as implants under load-bearing conditions [2, 3]. Typical materials used for the surgical implants are 316L stainless steels (316LSS), Co-Cr alloys, Co-Cr-Mo alloys, pure Ti and Ti-based alloys. However, a disadvantage of 316L stainless steels, Co-Cr and Co-Cr-Mo alloys is their high elastic modulus (E), closer to 200 GPa. Such E value is almost one order of magnitude higher than the E value of human bones, which is between 2 to 30 GPa [4]. Pure Ti and Ti based alloys have been widely employed in biomedical applications because of their relatively low E, low density, high specific strength, good biocompatibility and high corrosion resistance [5]. The first generation of Ti-based alloys has disadvantages such as relatively poor wear resistance, low hardness [6, 7] and toxicity due to constituent elements (Al, V Ni and Co) . These toxic elements have been reported to produce dermatitis, alzheimer, neuropathy and osteomalacia [8-10]. Another drawback for these first generation alloys is the elastic modulus mismatch between the Ti implant (~110 GPa) and human bone (2-30 GPa). An excessive elastic moduli affects the bones and produces a stress-shielding effect. Although a second generation of Ti-based alloys was developed with non-toxic elements for human body, such as Nb, Mo, Zr, Ta, Mn [11], they presented problems with their mechanical and corrosion properties. Current efforts are, in consequence, focused on finding new alloys with alloying elements suitable for biomaterial purposes [12].

Titanium has allotropy properties; exhibits a hexagonal closely packed (HCP) crystalline structure at room temperature, called α -phase, that changes to a body centered cubic (BCC) crystalline structure, called β -phase, when temperature exceeds 882°C. Mechanical properties of the α -phase and the β -phase are different; α -phase exhibits a good strength and creep resistance and β -phase exhibits high fatigue resistance and low elastic

modulus [12]. These characteristics make Ti-based alloys composed with β -phase and non-toxic elements a good candidate for biomaterials design. The β -phase can be stabilized at room temperature by adding alloying elements. Typical β stabilizers are Ta, Nb, Zr, W and Mo elements. However they exhibit high cost [13]. Some of the proposed alternative β -stabilizers of low cost are Mn, Fe, Cr and Sn elements [14]. Among them Mn is an essential element for the human body [15] and in recent years it has been reported that Mn has a special role in the formation of bone cartilage, bone collagen and bone mineralization as a co-factor [16]. At present, Ti-Mn alloys are mainly used in aerospace applications but have been poorly used in biomedical applications. Nicula et al. [17] have reported that Mn incorporation in Ti-Al-V alloys could enhance cell adhesion properties. Only few reports have studied the effect of Mn on Ti-based alloys, especially in the case of the second generation of Ti-based alloys, like Ti-13Nb-13Zr, Ti-35Nb-7Zr-5Ta, Ti-Mo, Ti-29Nb-13Ta-4.6Zr [14].

Ti-based alloys are usually fabricated by casting, forging and mechanical working [18]. A significant disadvantage associated with Ti-based alloys casting is that they become highly reactive at temperatures higher than 600°C and undergo rapid oxidation [13], which impose the use of special equipment such as high vacuum furnaces. Powder metallurgy (PM) process is a good way to synthesize Ti-based alloy because it makes possible to obtain net-shaped components and materials with a wide spectrum of properties [19]. An interesting PM processing technique is mechanical alloying (MA), which makes possible to produce Ti-based alloys with homogeneous composition and special microstructures that are difficult or impossible to achieve by casting, forging and mechanical working process [5]. MA is a non-equilibrium, simple and versatile process used to obtain advanced materials [20]. During MA, the powder particles are repeatedly flattened, cold welded, fractured and rewelded. The cold welding and fracturing processes can be predominant at any stage and depend mostly on the deformation characteristic of the starting powders and their kinetics. In MA, the energy is transferred from the balls to the powder during the milling cycle and produces large grain boundary surface area due to the decreased grain size and increased crystalline defects density. Furthermore, through MA process it is possible to obtain nanocrystalline and amorphous materials, which is of great interest because they exhibit an unusual combination of properties such as strength, ductility, high fracture toughness, and good corrosion resistance [21]. In contrast, coarse-grained materials lack of these chemical and physical properties [22]. Previous works reported that Ti-based alloys can be synthesized by MA in a wide range of compositions. Nazari et al. [23] studied the effect of compressive mechanical properties of Ti-10Nb-3Mo alloy with respect to the milling time.

These results showed that increasing milling time was beneficial for producing particle refinement and high alloying rate but at the cost of reducing their compressive mechanical properties. In that report yield strength changed from 1240 MPa to 730 MPa for 0 and 10 h of milling, respectively. Mahboubi Soufiani et al. [24] obtained Ti-6Al-4V nanocrystalline alloy with crystallite sizes between 20–50 nm. Zhuravleva et al. [25] synthesized Ti-40Nb and Ti-45Nb alloys with stabilized β -phase and concluded that these alloys can be used to produce metallic foams for orthopedic implants. Nouri et al. [19] synthesized Ti-16Sn-4Nb and demonstrated that the amount of process control agent changes the morphology and particle size distribution. In particular ball-milled particles with 1% stearic acid or ethylene bis-stearamide showed a relatively equiaxed shape with more symmetrical particle-size distribution. Long et al. [26] obtained ultrafine-grained Ti-6Al-4V powder using high energy ball milling. Corresponding TEM images analysis showed nanograins in a range between 12 and 30 nm. This work focuses on the synthesis of Ti-30Nb-13Ta-xMn (x: 2, 4 and 6 wt. %) alloys by MA using a shaker mill. The effects of Mn amount on the formation of solid solution and amorphous phase was investigated. In addition, the Gibbs free energy to form the solid solution and amorphous phase was calculated using theoretical models.

2 Materials and methods

In this work Ti-30Nb-13Ta-xMn alloys with composition x: 2, 4 and 6 wt.% Mn were studied. The characteristics of raw powders are given in table 1. The powder mixture was placed in a 65 ml hardened steel vial and milled in the SPEX 8000D mill in argon atmosphere. Also 1 wt% of stearic acid was added as a surfactant for milling process. Powders were milled for 2, 15 and 30 h using the hardened steel balls of 8.0 mm diameter. A constant ball/powder ratio of 10/1 was used. X-ray diffraction (XRD) analysis was performed in a Siemens D5000 diffractometer with copper target. All patterns were measured in an angular range between 30 and 120 degrees of 2θ with Cu-K α 1 radiation. Scanning electron microscopy SEM (Zeiss model EVO MA 10) was used to characterize size and morphology of milled powders. Transmission electron microscopy (TEM) measurements were performed using a FEI Tecnai of 200kV equipment. TEM samples were prepared by suspending powders in isopropyl alcohol and placing a drop on a Cu grid. Differential scanning calorimetry (DSC) studies were carried

out using a Texas Instruments Q20 calorimeter of continuous heating at 10 K/min rate up to reach 450 °C in an inert atmosphere.

Table 1. Characteristic of raw powders.

Powder	Purity	Size	Morphology	Company
Ti	Grade IV	-100 mesh, 149 μm	Irregular	GoodFellow
Nb	99.9%	-325 mesh, < 45 μm	Angular	NOAH Technologies Corporation
Ta	99.9%	-325 mesh, < 45 μm	Angular	GoodFellow
Mn	99.7	-100 to +320 mesh 149 to 45 μm	Angular	NOAH Technologies Corporation

3 Results and discuss

3.1 Characterization of as-received powders

Figure 1 shows the size and morphology of raw materials used in milling process. Ti powders exhibited a spongy aspect with size below 150 μm while Nb, Ta and Mn powders revealed irregular shape with sizes below 45 μm for Nb and Ta and below 150 μm for Mn. Ta powders exhibited the smaller particle size of all powders. In terms of morphology Nb and Mn samples showed particles with sharp edges whereas Ti and Ta samples exhibited particles with smooth edges. Ti particles were highly agglomerated, for this reason the particle size observed in figure 1(a) is larger compared with the size of other metallic powders.

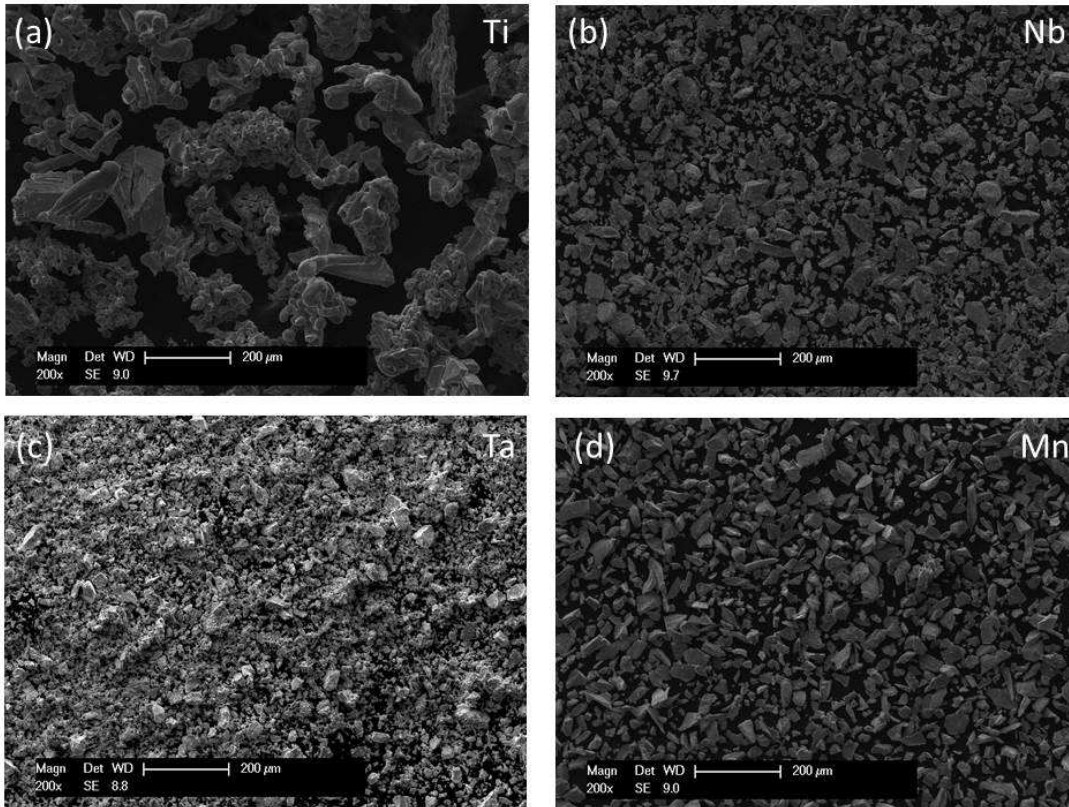


Figure 1. Morphology and size of raw powders, (a) titanium, (b) niobium, (c) tantalum and (d) manganese.

3.2 Characterization of milled powders

Figure 2 shows particle size of Ti-Nb-Ta-Mn alloy powders for different amounts of Mn and milling times. Observed particle size for 2%Mn alloy powder increased from $\sim 60 \mu\text{m}$ after 2 h of milling to $\sim 100 \mu\text{m}$ after 30 h of milling. In contrast, the 4 and 6%Mn alloy powder exhibited a reduction of particle size as milling time was increased. In the 4%Mn samples the particle size was reduced from $\sim 40 \mu\text{m}$ to $\sim 10 \mu\text{m}$ while in the 6%Mn samples was reduced from $\sim 80 \mu\text{m}$ to $\sim 30 \mu\text{m}$ for 2 and 30 h of milling, respectively. Agglomeration of particles was low for the 4 and 6% Mn alloy powder and high for the 2%Mn samples. In addition, observed particle morphology was irregular for 2 and 4 %Mn powders while it was more equiaxial for 6%Mn powders for all milling times. These results indicate Mn content influences the resulting morphology of milling process products. Large roughness of particle edges in 2 and 6%Mn samples indicates that the fracture process was more relevant than

cold welding. Conversely, particle edges of 4%Mn samples were smoother, indicating the predominance of cold welding over fracture process for this Mn content (figure 3). In MA the energy transferred from the balls to the powder during the milling process produces large grain boundary surface area (reduced grain size) and high crystalline defect density. The newly created surface enables the particles to weld together which leads to an increase in agglomeration of particles [20]. As the milling time and amount of Mn increases, Mn atoms are more prone to enter into the solid solution producing higher strain and promoting the fracture, which result in the observed particle size decrease. For long milling time the powder particles get work hardened which increases their hardness and brittleness whereas the particle size keep decreasing when the fracture strength of the particles are equal or smaller than the stress caused by the collision. On another hand, if the milling time increases the level of contamination in the milled powders increases as well. EDS analysis detected the presence of O and Fe in samples after 15 and 30 h of milling. The observed milled powder contamination can be attributed to two sources: i) the hardened steel vials and balls and ii) the decomposition of stearic acid which introduces carbon and oxygen contamination to the powder particles [20].

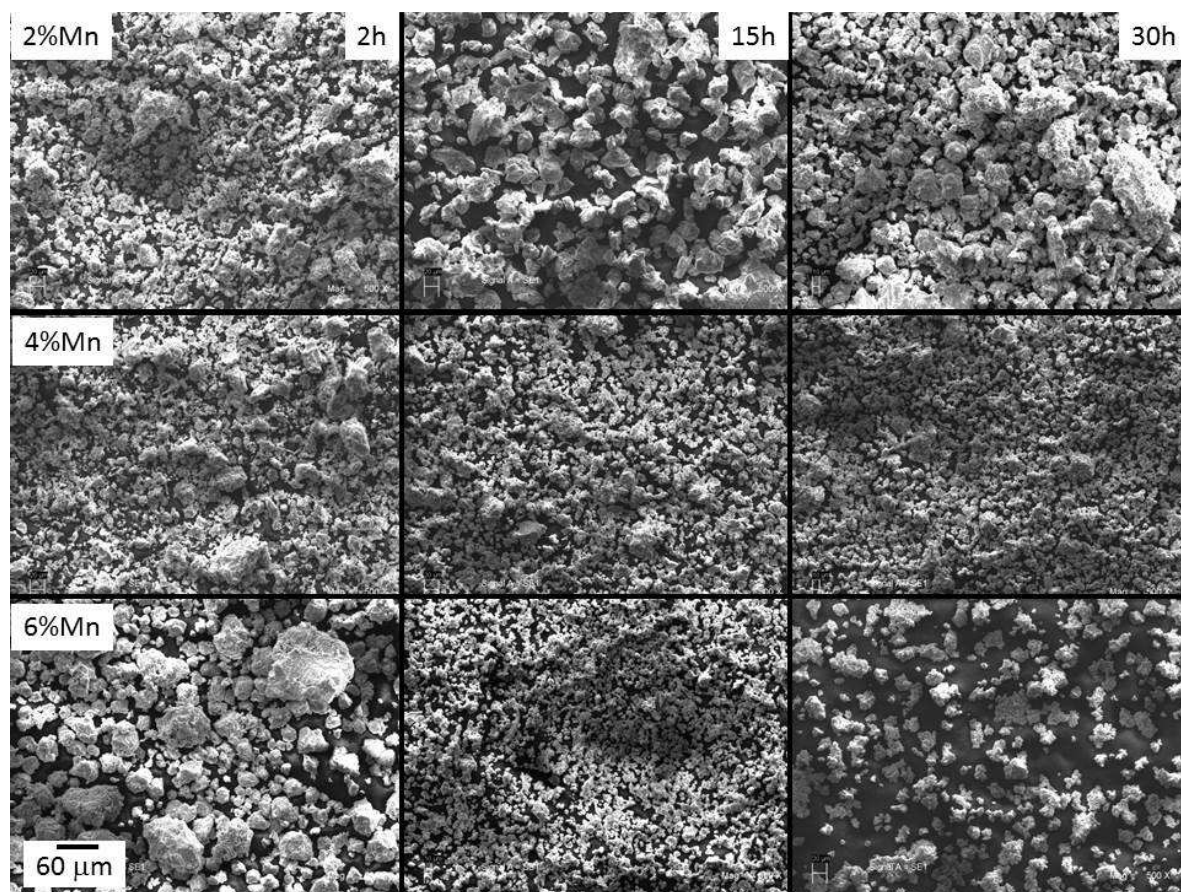


Figure 2. SEM images (500X) of milled powders of Ti-30Nb-13Ta-xMn (x: 2, 4, 6 wt%) alloys.

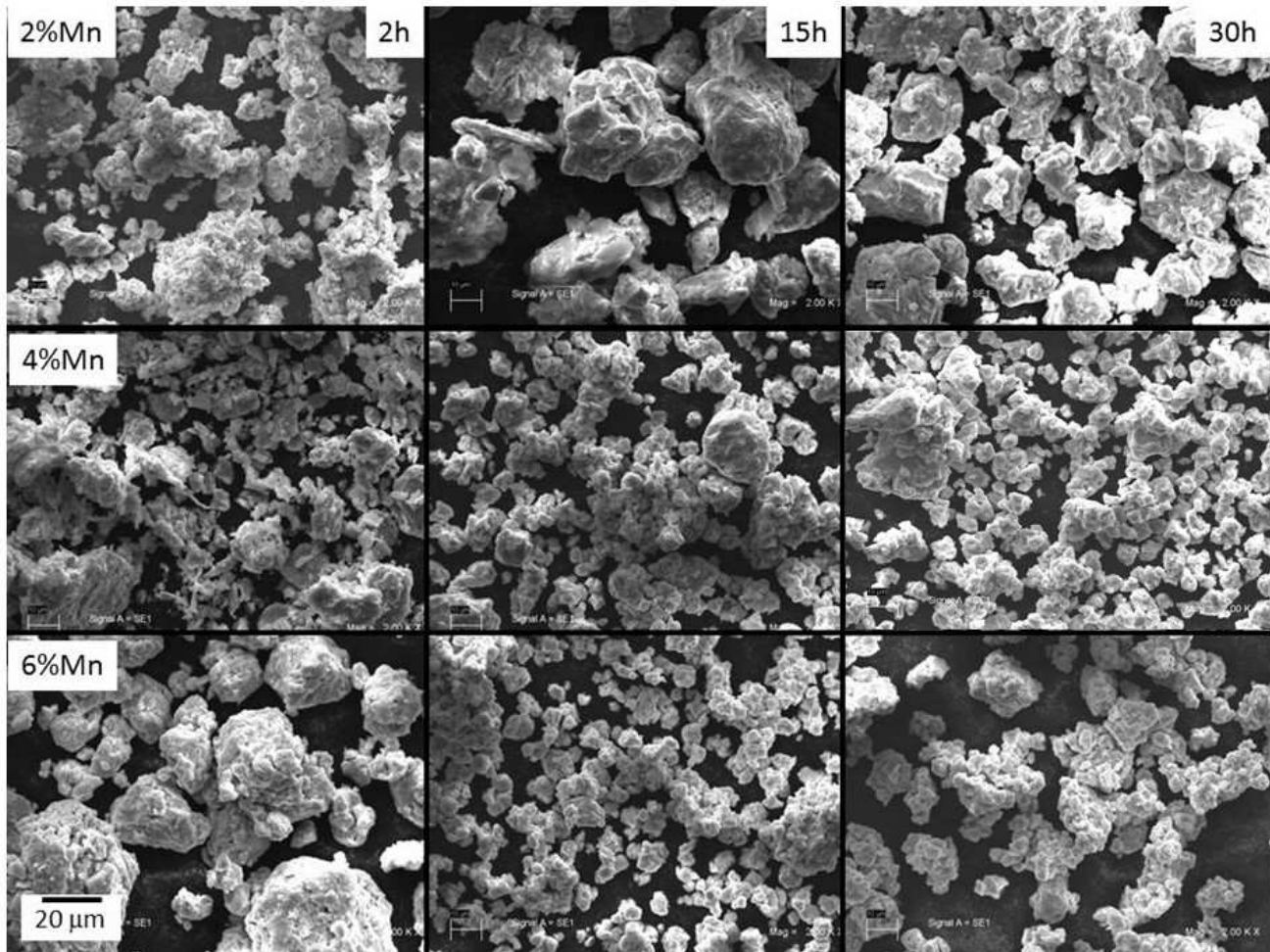


Figure 3. SEM images (2000X) of milled powder of Ti-30Nb-13Ta-xMn (x: 2, 4, 6 wt%) alloys.

Figure 4 shows the X-ray diffraction patterns of powders milled for 2, 15 and 30 h. The XRD patterns exhibited the typical behavior of powders processed by MA such as peak broadening, peak shift and disappearance of peaks of solute due to a severe plastic deformation. The strongest Nb (110) and (211) peaks are detected at $2\theta=38.6$ and 70.2 [27], the strongest Ta (110) and (211) peaks at $2\theta=38.6$ and 69.5 [27] and the strongest Mn (221), (310) and (510) peaks are at $2\theta=43.0$, 45.3 and 76.8 [27], respectively. Ti- β phase, Nb, Ta and Mn have same crystalline structures and space group; $Im-3m$. For this reason observed X-ray peaks are very close in 2θ values, as it is clearly shown in figure 4 for 2h milling time. For all alloys, the strongest Nb, Ta and Mn peaks were found for 2h milling time and disappeared for 15 and 30 h of milling time. The disappearance of Nb, Ta and

Mn peaks it is considered to be related to the formation of a solid solution [20]. After 2 h of milling, two types of titanium were observed; Ti- α (hexagonal crystalline structure with a space group P63/mmc) and Ti- β . When milling time increased, the Ti- α disappeared whereas the Ti- β remained due to the presence of Nb, Ta and Mn that act as β -stabilizing agents (they form solid solution with Ti).

In addition, milling times increase crystalline defect density, decreasing crystallite size and increasing dislocations, stacking faults, twins, and vacancies [20], which leads to peak broadening. All XRD patterns exhibited broad peaks after 15 and 30 h of milling due to the high density of crystalline defects. 6%Mn powders milled for 30h exhibited a mixing of a partially amorphous hump and a nanocrystalline phase as is observed in figure 4c for 2θ values between 35 to 45°. Through MA, it is possible to produce amorphous phases [28] with composition ranges wider than any other processes (far from the eutectic temperature) [29]. Another characteristic of MA, is that it makes possible to form amorphous phases from elemental powders with positive heat of mixing [30]. The mechanism of amorphous phase production by MA is different than the one associated to liquid-quenching techniques. The solid solution and the strain energy increases linearly with the solute content. If the lattice strain reaches a critical value, the formation of an amorphous phase becomes more favorable than formation of a crystalline phase. During MA, the powder suffers by severe plastic deformation which produces high crystalline defect density and increases grain boundary area, promoting a faster diffusion process [31] due from the smaller atomic volume ratio, which leads to the amorphous phase formation [32, 33]. The requirements for the amorphous phase formation are different than the corresponding ones for liquid-quenching techniques [34] and solid-state processing techniques such as MA [35]. A typical requirement for the amorphous phase formation using any of these techniques is that there must be a significant difference in atomic sizes between the constituent elements, which introduces large strain into the alloy [36]. The atomic radius of Ti, Nb and Ta are similar, but different when compared to the atomic radius of Mn. The atomic sizes of Ti, Nb, Ta and Mn are 0.2, 0.208, 0.209 and 0.179 nm, respectively [37].

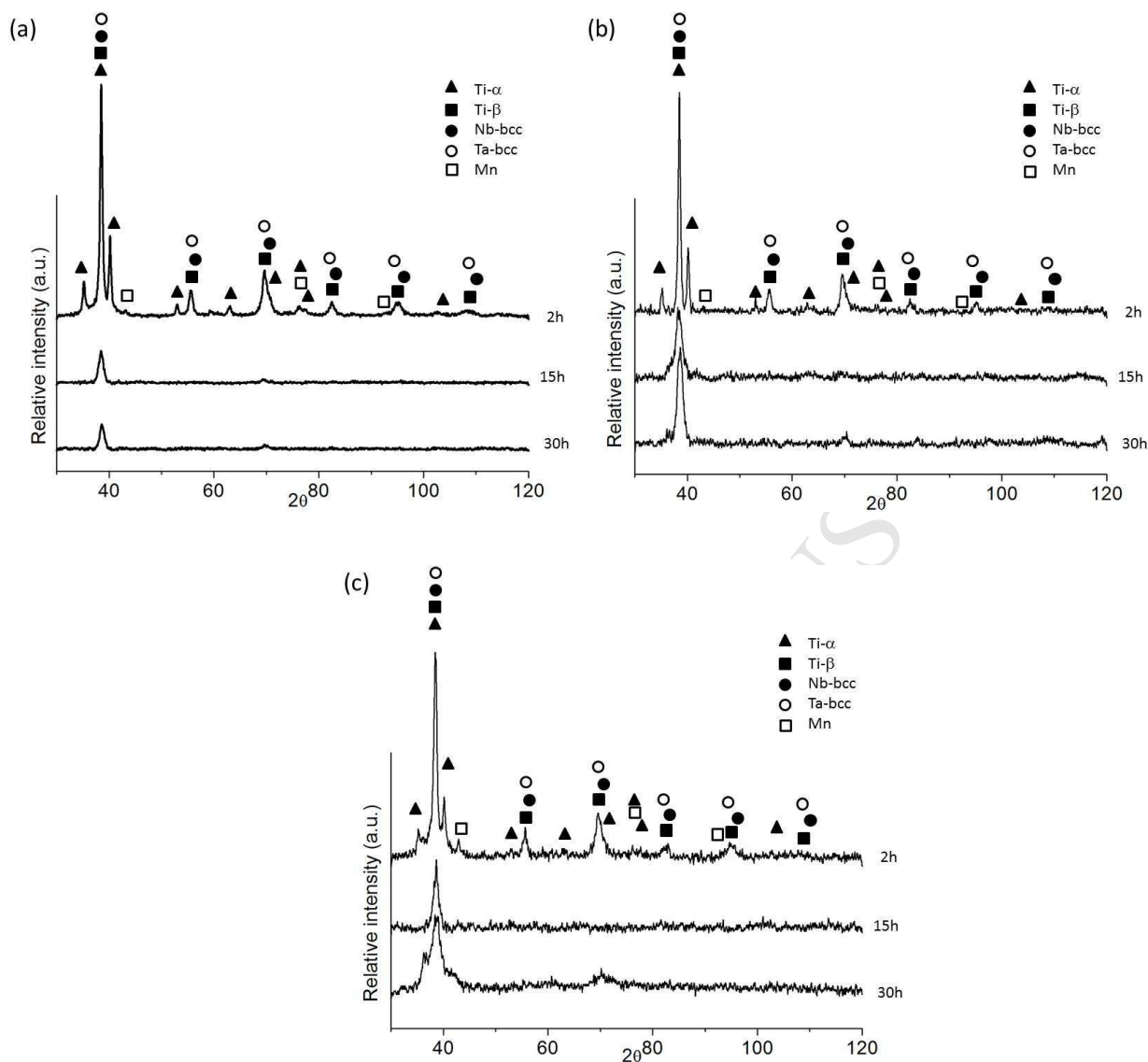
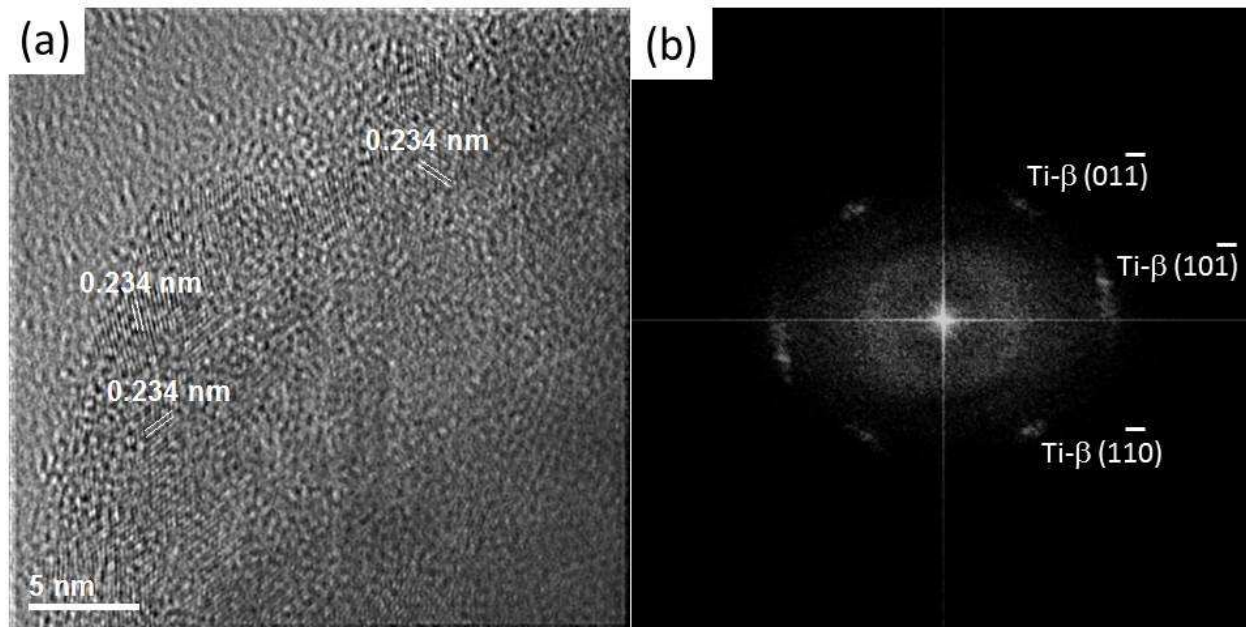
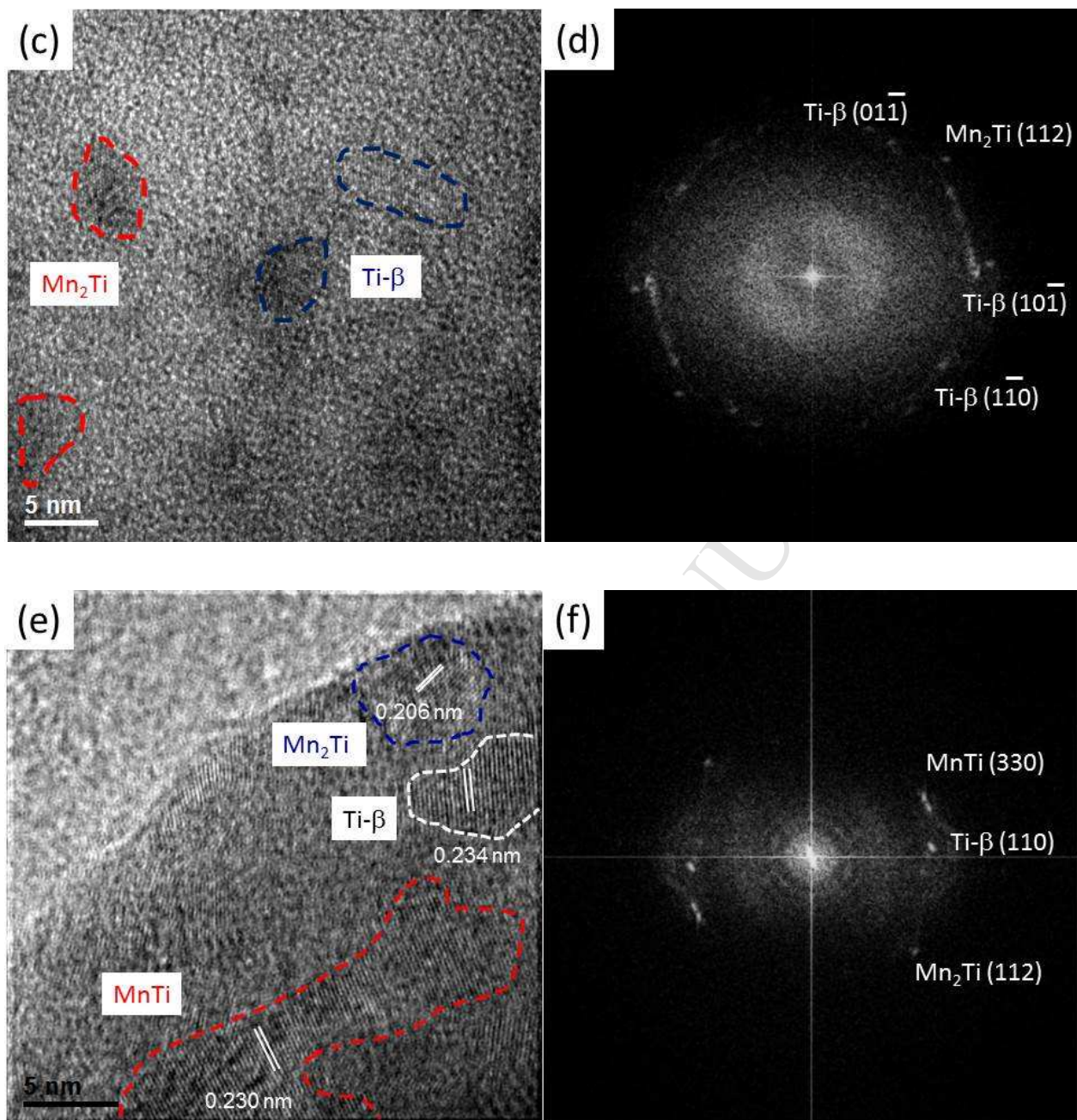


Figure 4. XRD pattern of milled powder, (a) Ti-30Nb-13Ta-2Mn, (b) Ti-30Nb-13Ta-4Mn and (c) Ti-30Nb-13Ta-6Mn as a function of milling time.

Figure 5 shows high resolution TEM (HRTEM) images of the milled powders. The images confirmed the presence of mixed zones of nanocrystalline and amorphous phases for all the alloys. The alloy with 6%Mn exhibited more extended amorphous phases (figure 5g and i), which is in agreement with XRD results shown in figure 4. Ti- α and Ti- β phases were detected in all alloys, although the presence of Ti- α decreased with milling time because Nb, Ta and Mn acted as β -stabilizing agents that determine solid solution formation. Also,

nanocrystalline particles of intermetallic compounds were detected. Figure 5c shows the Mn_2Ti nanoparticle embedded in the Ti-30Nb-13Ta-2Mn alloy milled for 15 h whereas figure 5d shows the corresponding fast Fourier Transform (FFT). The observed Mn_2Ti nanoparticles size was around 5 nm. Figure 5e shows the two MnTi and Mn_2Ti nanoparticles embedded in the same alloy milled for 30h, with the corresponding FFT in figure 5f. The MnTi and Mn_2Ti nanoparticles size were around 35 and 8 nm, respectively. Finally figure 5i shows NbTi_4 and MnTi nanoparticles in the Ti-30Nb-13Ta-6Mn alloy milled for 30 h with the corresponding FFT in figure 5j. The MnTi and NbTi_4 nanoparticles size was 30 and 5 nm, respectively. The absence of nanoparticles for 2h milling process indicates that such nanostructured compound required higher milling times to be formed. MnTi, an intermetallic compound, and Mn_2Ti , a phase, are present in the equilibrium phase diagram of the Ti-Mn system [38]. NbTi_4 is a non-equilibrium compound that is not present in the phase diagram of equilibrium of the Ti-Nb system [38].





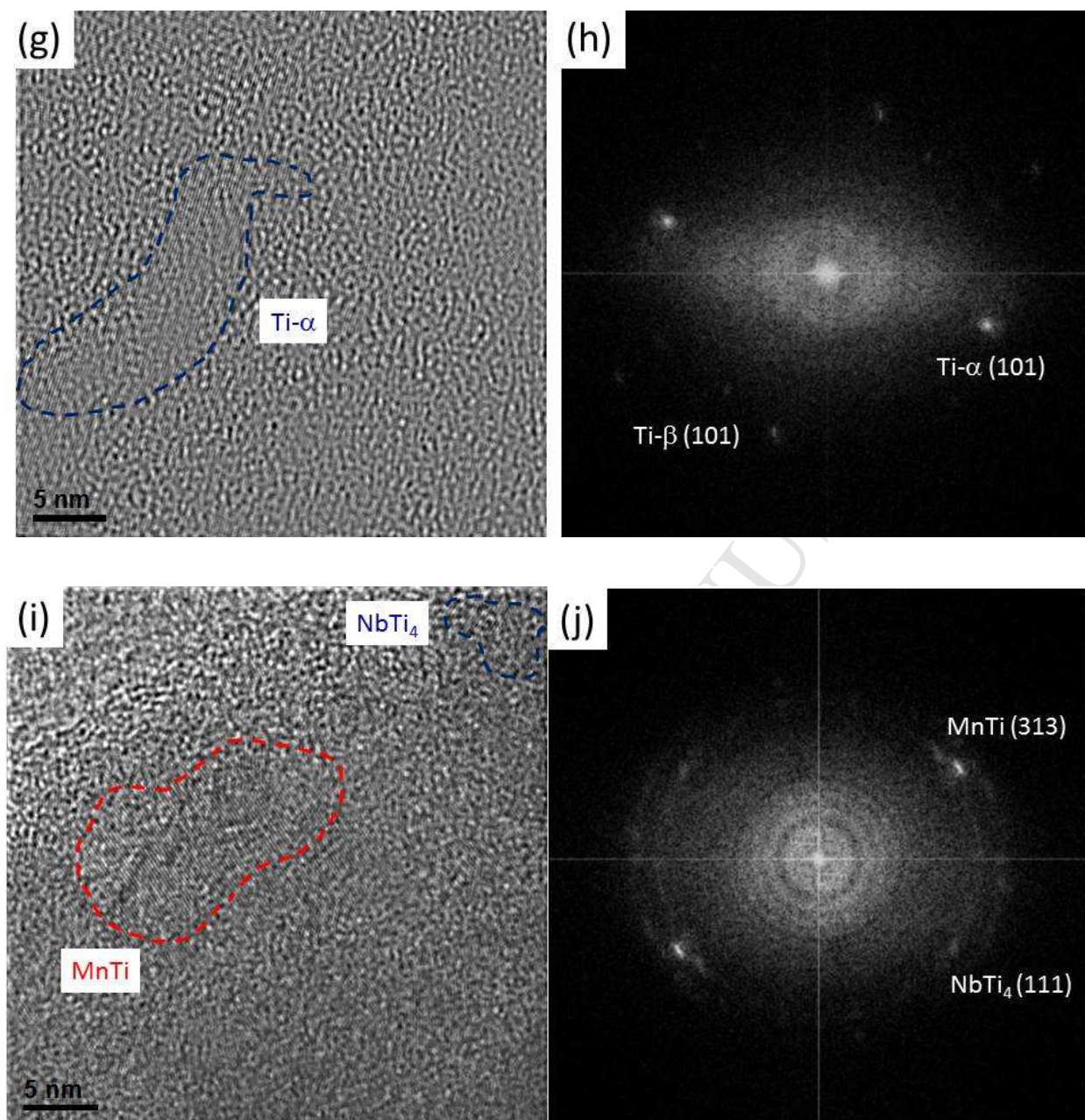


Figure 5. HRTEM images, (a)-(b) Ti-30Nb-13Ta-2Mn, 2h of milling, (c)-(d) Ti-30Nb-13Ta-2Mn, 15h of milling, (e)-(f) Ti-30Nb-13Ta-4Mn, 30h of milling, (g)-(h)-(i)-(j) Ti-30Nb-13Ta-6Mn, 30h of milling.

Figure 6 shows the DSC normalized curves of milled powders. The curves exhibited a broad exothermic event that began at 200 °C for three alloys. This event corresponds to the continuous recrystallization of amorphous phase. The alloys with higher amount of Mn showed the first recrystallization events as a function of temperature. In addition, the required energy for the recrystallization process of Ti-30Nb-13Ta-6Mn alloy is higher than the required for Ti-30Nb-13Ta-4Mn and Ti-30Nb-13Ta-2Mn alloys. Zhernovenkova et al. [39] reported similar behavior for the recrystallization of the amorphous phase of Ti-Ni-Zr alloys produced by MA.

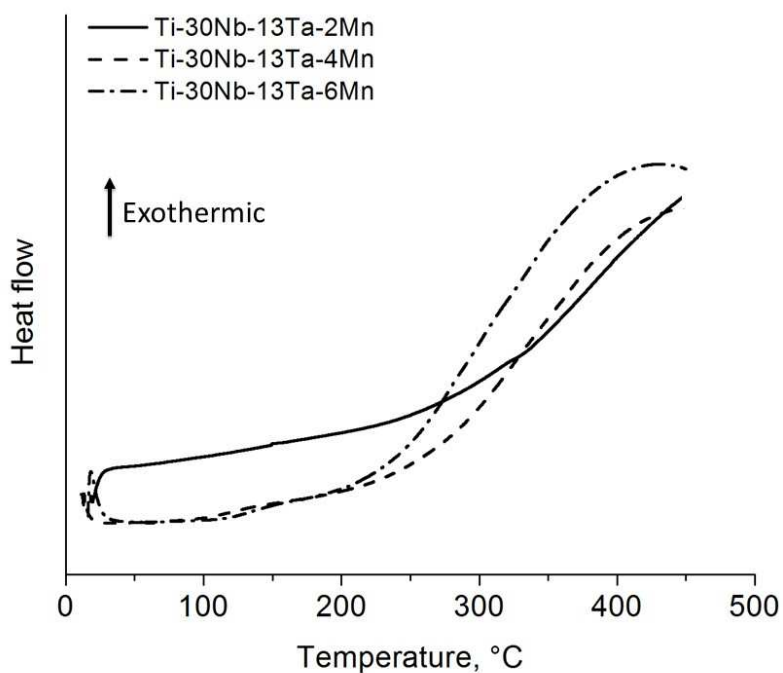


Figure 6. DSC curves of Ti alloys milled 30 h.

3.2 Thermodynamics analysis

There are only a few reports on the thermodynamic properties of ternary and quaternary systems composed by Ti, Nb, Ta and Mn. Multi-component characteristic of these systems makes very difficult to obtain their thermodynamic information by experimental measurements, in most of the cases. In this context, the theoretical calculations are excellent tools to estimate thermodynamic properties of these systems. A general approach to

obtain thermodynamic information of ternary systems is the extrapolation of constitutive binary systems. Some extrapolation methods used to obtain ternary systems were proposed by Toop's [40], Wang's [41], Kohler [42], Manasijevic et al. [43], Redlich et al. [44], Hoch [45]. The use of theoretical models is a widely known and relatively simple method to obtain the thermodynamic properties of binary systems. Through applying Miedema and Baker's models [46, 47] it is possible to obtain enthalpy of mixing and Gibbs free energy of mixing. In order to obtain thermodynamic properties in ternary systems it is necessary to apply any extrapolation method. Extrapolation of ternary systems have given reasonable results [48-50], but in the case of quaternary systems such methods still need more investigation. For this reason, only the thermodynamic analysis of ternary systems was considered in this work. The systems considered were Ti-Nb-Ta, Ti-Nb-Mn and Ti-Ta-Mn.

The Gibbs free energy changes due to disordering A(B) solid solution formation from a mixing of pure elements A and B. This expression can be defined by eq. 3, where ΔH^m and ΔS^m are the enthalpy and entropy of mixing and T is the temperature of solid solution formation.

$$\Delta G^m = \Delta H^m - T\Delta S^m \quad (3)$$

The energy of any system composed by atoms is composed of vibrational, rotational, translational, nuclear and chemical energies. In this work it was assumed that the contribution of chemistry source is the largest one. If only configurational entropy is considered, the entropy of mixing can be computed using Eq. (4), where R is the universal gas constant and x_i are the mole fractions of element i. On the other hand the enthalpy of mixing can be obtained as the sum of three terms in Eq. (5), where $\Delta H_{\text{chemical}}$ is the chemical contribution of creation and breaking of atomic bonds, $\Delta H_{\text{elastic}}$ is the elastic contribution (elastic mismatch energy) in solid solutions and $\Delta H_{\text{structural}}$ is the contribution of lattice stability energy due to the differences in valence electrons, crystal structure of solute and solvent atoms.

$$\Delta S^m = R \sum_{i=1}^n x_i \ln x_i \quad (4)$$

$$\Delta H^m = \Delta H_{\text{chemical}} + \Delta H_{\text{elastic}} + \Delta H_{\text{structural}} \quad (5)$$

The chemical contribution can be estimated by applying the model proposed by Miedema [46, 47] which is widely used because of its simplicity. The $\Delta H_{\text{chemical}}$ for each binary system can be determined by means of eq. 6, where V_A , V_B are the molar volumes of atoms A and B, respectively, ϕ^* is the work function of constituent elements, n_{ws} is the electron density, P, Q and R' are constants related to constituent elements and $f(C^S) = C_A^S C_B^S$, where C_A^S and C_B^S are determined by eq. 7. Differences between enthalpy of mixing obtained from Miedema's model and experimental data have been reported. Wang et al. [49] proposed a correction factor $S(x)$ (eq. 8) which takes into account the atomic size of solvent and solute atoms, where C is an empirical parameter that describes the effect of atomic size differences in a semi-quantitative manner. C is considered equal to 0.5 and 2.0 for the liquid alloy and ordered compound, respectively. For a disordered solid solution C is considered equal to 1.

$$\Delta H_{\text{chemical}} = 2Pf(C^S)S(x) \frac{(x_A V_A^{2/3} + x_B V_B^{2/3})}{(n_{\text{ws}}^A)^{-1/3} + (n_{\text{ws}}^B)^{-1/3}} x \left[-(\Delta\phi^*)^2 + \frac{Q}{P} (\Delta n_{\text{ws}}^{1/3})^2 - \frac{R'}{P} \right] \quad (6)$$

$$C_A^S = \frac{x_A V_A^{2/3}}{x_A V_A^{2/3} + x_B V_B^{2/3}} \quad C_B^S = \frac{x_B V_B^{2/3}}{x_A V_A^{2/3} + x_B V_B^{2/3}} \quad (7)$$

$$S(x) = 1 - C \frac{x_A x_B |V_A - V_B|}{x_A^2 V_A + x_B^2 V_B} \quad (8)$$

The $\Delta H_{\text{elastic}}$ can be calculated by the expression proposed by Bakker et al. [51] (eq. 9), where $\Delta E_{A \text{ in } B}$ is the elastic mismatch energy caused by the element A dissolved in the element B and $\Delta E_{B \text{ in } A}$ is the elastic mismatch energy caused by the element B dissolved in the element A. $\Delta E_{i \text{ in } j}$ values can be calculated using eqs. 10, where K , and G are the bulk and shear modulus, respectively.

$$\Delta H_{\text{elastic}} = x_A x_B (x_A \Delta E_{A \text{ in } B} + x_B \Delta E_{B \text{ in } A}) \quad (9)$$

$$\Delta E_{A \text{ in } B} = \frac{2K_A G_B (V_B - V_A)^2}{3K_A V_B + 4G_B V_A} \quad \Delta E_{B \text{ in } A} = \frac{2K_B G_A (V_A - V_B)^2}{3K_B V_A + 4G_A V_B} \quad (10)$$

Finally, $\Delta H_{\text{structural}}$ is a small positive value and it can be neglected in the estimation of enthalpy of mixing. The required parameters to solve the equations are listed in table 1.

Table 1. Parameters for thermodynamic analysis of Ti, Nb, Ta and Mn [46].

Parameters	Ti	Nb	Ta	Mn
$n_{ws}^{1/3} (\text{cm}^{-1})$	1.47	1.62	1.63	1.61
$\Phi^* (V)$	3.65	4.00	4.05	4.45
$K (10^{10} \text{ Nm}^{-2})$	11	17	20	12
$G (10^{10} \text{ Nm}^{-2})$	4.4	3.8	6.9	1.7
$V (\text{cm}^3 \text{ mol}^{-1})$	4.8	4.9	4.9	3.8
$T^m (K)$	1358	2130	2890	1517
$P (\text{kJV}^{-2} \text{ cm}^{-1})$	14,1			
$Q (\text{kJV}^{-1})$	132,54			
R'/P	0			

The extension of Midema's model to ternary systems can be determined in based of two kind of models; symmetrical [52] and asymmetrical [40]. Asymmetrical model considers the effect of a third element and avoids the large deviation of calculated values from experiment when constituent elements have different physical properties. To obtain ΔH^m for the ternary system, $\Delta H_{\text{chemical}}$ and $\Delta H_{\text{elastic}}$ of the binary systems need to be individually calculated. $\Delta H_{\text{chemical}}$ and $\Delta H_{\text{elastic}}$ values of the ternary systems are obtained through interpolation methods, applying the Toop's model given by eq. 11 [40], where ΔH_{A-B}^m , ΔH_{B-C}^m , ΔH_{C-A}^m are the mixing enthalpies of three binary systems. ΔH_{ij}^m is the chemical and the elastic contributions of the binary system. The A, B and C terms can be Ti, Nb, Ta or Mn indistinctly.

$$\Delta H^m = \left(\frac{x_B}{x_A + x_B} \right) \Delta H_{A-B}^m (x_A, 1-x_A) + \left(\frac{x_C}{x_A + x_C} \right) \Delta H_{A-C}^m (x_A, 1-x_A) + (x_B + x_C)^2 \Delta H_{B-C}^m \left(\frac{x_B}{x_B + x_C}, \frac{x_C}{x_B + x_C} \right) \quad (11)$$

During MA the crystalline defect density in metallic powders increases due to the severe plastic deformation. In some systems, these defects increase internal energy making energetically favorable for the crystal to be amorphous. The enthalpy of amorphization (ΔH^{am}) can be calculated by eq. 12 [53], where $\alpha = 3,5 \text{ Jmol}^{-1}$ and $T_{fuse} = x_A T_A^m + x_B T_B^m$, T^m is the melting temperature of A and B elements.

$$\Delta H^{am} = \Delta H_{\text{chemical}} + \alpha T_{fuse} \quad (12)$$

Figure 7a, b and c shows the calculated Gibbs free energy of mixing (ΔG^m) for the formation of solid solutions of Ti-Nb-Ta, Ti-Nb-Mn and Ti-Ta-Mn ternary systems, whereas figure 6d, e and f display Gibbs free energy (ΔG^{am}) for the formation of amorphous phase of the same ternary systems. The ΔG^m and ΔG^{am} values were obtained using the equations $\Delta G^m = \Delta H^m + T\Delta S^m$ and $\Delta G^{am} = \Delta H^{am} + T\Delta S^m$ (only configurational entropy was considered in the ΔS^m term). The ΔG^m and ΔG^{am} values for ternary systems were obtained by solving eq. 11 at room temperature. Figures are expressed in at.%, therefore, it was necessary to convert the chemical composition of alloys from wt.% to at.%. Considering this, the corresponding composition is Ti-21Nb-5Ta-xMn ($x = 2, 5$ and 7 , at.%). The amount of Ti changes from 67 to 73 at.% depending on the amount of Mn. The Gibbs free energy to form solid solutions is negative in the whole composition range for the three ternary systems at room temperature, as is shown in figures 7a, b and c. This result indicates that a driving force is required to form solid solution from elemental Ti, Nb, Ta and Mn powders. This is in agreement with the reported information of binary phase diagrams for Ti-Nb, Ti-Ta and Ti-Mn [54]. The ΔG^m values to form Ti-Nb-Mn and Ti-Ta-Mn solid solutions are very similar and more negative compared with the corresponding ΔG^m values for the Ti-Nb-Ta system. The exact ΔG^m values are difficult to obtain from figure 7 because the alloys contain four elements, but a general analysis of the characteristic of the systems can be performed. Some common features in figures 6a, b and c are: i) corners of triangles have higher ΔG^m values compared with values at the center of the triangles, (ii) All ΔG^m values in the figures were negative indicating that the solid solutions can be formed in the whole composition range (at room temperature) and iii) the smaller ΔG^m values to form solid solution were close to the center of the triangles. These ΔG^m values were around of -4.0 kJ mol^{-1} , 9.5 kJ mol^{-1} and 9.0 kJ mol^{-1} for the Ti-Nb-Ta, Ti-Nb-Mn and Ti-Ta-Mn systems, respectively. Figures 7d, e and f, show the Gibbs free energy needed

to form an amorphous phase for the same ternary systems. It is observed that ΔG^{am} is positive in the whole composition range, which means that the formation of amorphous phase requires an external energy. There is no driving force to form amorphous phase from elemental powders (in any of the studied systems). Some common characteristics of the Gibbs free energy diagrams for the formation of amorphous phase in figures 7d, e and f are: i) higher ΔG^{am} values were found at the Ta or Nb corners and ii) smaller ΔG^{am} values were found when Mn was added. The smallest calculated ΔG^{am} values were around of 10, 1.5 and 1.1 kJ mol^{-1} for the Ti-Nb-Ta, Ti-Nb-Mn and Ti-Ta-Mn systems, respectively. The maximum calculated ΔG^{am} values were around 20 kJ mol^{-1} at the corners of Ta and Nb, while the ΔG^{am} values were smaller at the Mn corner. In addition, ΔG^{am} values decrease when the amount of Mn increases and when Ta decreases (or is not present) (figure 7d with figures 7e and f). By using a shaker mill it is possible to store high values of energy, over 16 kJ mol^{-1} for the metallic powder. Aguilar et al. [48] estimated that the stored energy values for shaker milled Cu-Cr-Mo powders are between 10 and 20 kJ mol^{-1} . If the difference in atomic radii of the constituent elements is high then a high strain will be introduced into the alloy leading to the formation of an amorphous phase [36]. The difference in atomic radius between Ti, Nb and Ta is around 0.001-0.009 nm, which is a small value when compare to the 0.021-0.03 nm corresponding to the difference between Ti, Nb, Ta and Mn. The elastic contribution to the enthalpy mixing for Mn is larger due to the difference between K, G and V values of Mn and Ti, Nb and Ta. The Gibbs free energy mixing required to form solid solution is smaller than the required to form an amorphous phase for the three ternary systems. Therefore, the ternary systems always form the solid solutions first, and then the amorphous phase will be formed if continuous milling is applied. During MA, the intense deformation introduced into the particles increases crystallite boundaries and crystalline defects, such as dislocation and stacking faults. When lattice strain reaches a critical value, the amorphous phase formation becomes more favorable than the crystalline phase. The thermodynamic data are in agreement with the XRD and TEM data (figure 4 and 5, respectively). For 2 and 15 h of milling the strongest peaks of Nb, Ta and Mn disappear indicating the formation of solid solution. For 30 h of milling almost all peaks disappeared and only the strongest peak of Ti was observed, exhibiting a high broadening with an amorphous hump. This behavior becomes more evident when the amount of Mn is increased.

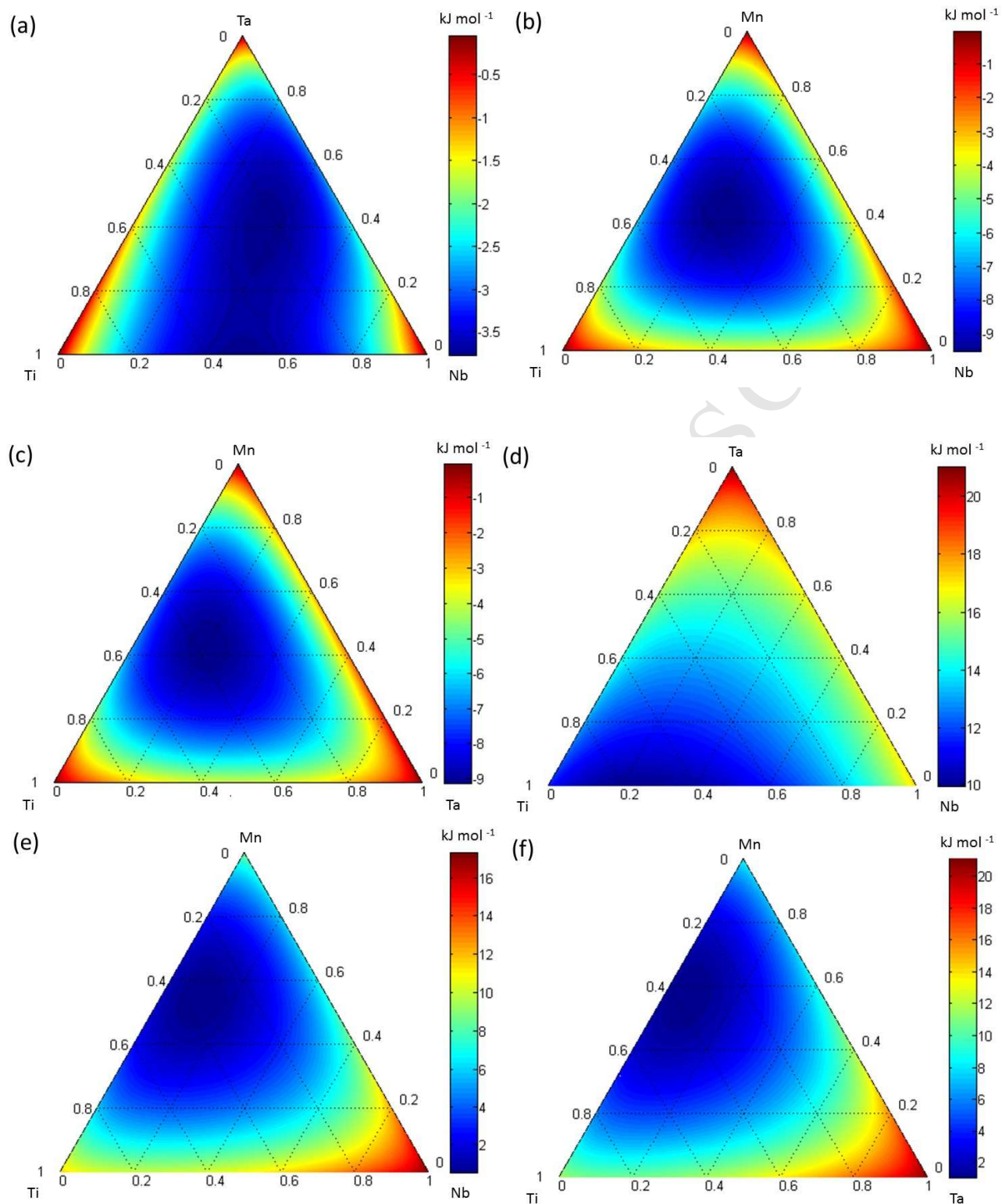


Figure 7. Gibbs free energy of mixing for the formation of solid solutions of (a) Ti-Nb-Ta, (b) Ti-Nb-Mn and (c) Ti-Ta-Mn, Gibbs free energy for the formation of amorphous phase (d) Ti-Nb-Ta, (e) Ti-Nb-Mn and (f) Ti-Ta-Mn.

4 Conclusions

The disappearance of Nb, Ta and Mn strongest peaks in the X-ray pattern of powders milled for 15 h indicates that a solid solution between Ti and such elements can be formed by mechanical alloying. In addition, TEM measurements confirmed that nanocrystalline intermetallic compounds were formed during MA process. The compounds detected by TEM images analysis were Mn_2Ti , $MnTi$ and $NbTi_4$, with size ranging from 3 to 20 nm.

From the XRD and TEM analysis the formation of an amorphous phase was detected in the 6%Mn alloy milled for 30 h. In addition, embedded nanoparticles of the intermetallic compounds in a nanocrystalline phase were found in all alloys. The energy provided by the MA process was large enough to give rise to an amorphous phase formed by Ti, Nb, Ta and Mn.

The approach used to obtain and analyze the thermodynamic properties of Ti-Nb-Ta-Mn system are in agreement to XRD and TEM results. Experimental and thermodynamic data showed that solid solution was formed in a first stage followed by the formation of an amorphous phase, as the milling time increased. The Gibbs free energy values to form solid solutions of the ternary systems Ti-Nb-Ta, Ti-Nb-Mn and Ti-Ta-Mn are negative in the whole composition range. In contrast, the Gibbs free energy values to form amorphous phase are positive in the whole composition range and decrease from 20 kJ mol^{-1} in the corners rich in Ta and Nb to 2 kJmol^{-1} when Mn is added to the ternary system. Therefore, the presence of Mn promotes the formation of an amorphous phase due to the large atomic radius difference between Ti, Nb, Ta and Mn (the atomic radius of Ti, Nb and Ta are similar).

Acknowledgments

The authors would like to acknowledge financial support from FONDECYT project n° 1130417.

5 References

- [1] M. Geetha, A.K. Singh, R. Asokamani, A.K. Gogia, Ti based biomaterials, the ultimate choice for orthopaedic implants – A review, *Progress in Materials Science*, 54 (2009) 397-425.
- [2] M. Niinomi, Recent research and development in titanium alloys for biomedical applications and healthcare goods, *Science and Technology of Advanced Materials*, 4 (2003) 445-454.
- [3] J. Xiong, Y. Li, X. Wang, P. Hodgson, C.e. Wen, Mechanical properties and bioactive surface modification via alkali-heat treatment of a porous Ti–18Nb–4Sn alloy for biomedical applications, *Acta Biomaterialia*, 4 (2008) 1963-1968.
- [4] N. Nomura, T. Kohama, I.H. Oh, S. Hanada, A. Chiba, M. Kanehira, K. Sasaki, Mechanical properties of porous Ti–15Mo–5Zr–3Al compacts prepared by powder sintering, *Materials Science and Engineering: C*, 25 (2005) 330-335.
- [5] A. Nouri, X. Chen, Y. Li, Y. Yamada, P.D. Hodgson, C.e. Wen, Synthesis of Ti–Sn–Nb alloy by powder metallurgy, *Materials Science and Engineering: A*, 485 (2008) 562-570.
- [6] X. Liu, P.K. Chu, C. Ding, Surface modification of titanium, titanium alloys, and related materials for biomedical applications, *Materials Science and Engineering: R: Reports*, 47 (2004) 49-121.
- [7] G. Lütjering, J.C. Williams, *Titanium*, Springer, 2003.
- [8] K.L. Wapner, Implications of metallic corrosion in total knee arthroplasty, *Clinical orthopaedics and related research*, 271 (1991) 12-20.
- [9] S. Nag, R. Banerjee, H.L. Fraser, Microstructural evolution and strengthening mechanisms in Ti–Nb–Zr–Ta, Ti–Mo–Zr–Fe and Ti–15Mo biocompatible alloys, *Materials Science and Engineering: C*, 25 (2005) 357-362.
- [10] E. Eisenbarth, D. Velten, M. Müller, R. Thull, J. Breme, Biocompatibility of β -stabilizing elements of titanium alloys, *Biomaterials*, 25 (2004) 5705-5713.
- [11] E.B. Taddei, V.A.R. Henriques, C.R.M. Silva, C.A.A. Cairo, Production of new titanium alloy for orthopedic implants, *Materials Science and Engineering: C*, 24 (2004) 683-687.
- [12] A. Biesiekierski, J. Wang, M. Abdel-Hady Gepreel, C. Wen, A new look at biomedical Ti-based shape memory alloys, *Acta Biomaterialia*, 8 (2012) 1661-1669.
- [13] M. Chandrasekaran, Z.S. Xia, Effect of alloying time and composition on the mechanical properties of Ti alloy, *Materials Science and Engineering: A*, 394 (2005) 220-228.
- [14] M. Niinomi, M. Nakai, J. Hieda, Development of new metallic alloys for biomedical applications, *Acta Biomaterialia*, 8 (2012) 3888-3903.
- [15] A. Ibrahim, F. Zhang, E. Otterstein, E. Burkel, Processing of porous Ti and Ti5Mn foams by spark plasma sintering, *Materials & Design*, 32 (2011) 146-153.
- [16] S.E. Brown, *Bone nutrition: Scientific evidence for musculoskeletal, bariatric, and sport nutrition.*, CRC Press, 2006.
- [17] R. Nicula, F. Lüthen, M. Stir, B. Nebe, E. Burkel, Spark plasma sintering synthesis of porous nanocrystalline titanium alloys for biomedical applications, *Biomolecular Engineering*, 24 (2007) 564-567.
- [18] T. Grosdidier, M.J. Philippe, Deformation induced martensite and superelasticity in a β -metastable titanium alloy, *Materials Science and Engineering: A*, 291 (2000) 218-223.
- [19] A. Nouri, P.D. Hodgson, C.E. Wen, Effect of process control agent on the porous structure and mechanical properties of a biomedical Ti–Sn–Nb alloy produced by powder metallurgy, *Acta Biomaterialia*, 6 (2010) 1630-1639.
- [20] C. Suryanarayana, Mechanical alloying and milling, *Progress in Materials Science*, 46 (2001) 1-184.
- [21] C. Suryanarayana, *Non-equilibrium processing of materials*, Elsevier, 1999.
- [22] T.T. Tsong, Design and characterization of materials on the atomic scale, *Materials Science and Engineering: A*, 286 (2000) 87-90.
- [23] K.A. Nazari, A. Nouri, T. Hilditch, Effects of milling time on powder packing characteristics and compressive mechanical properties of sintered Ti-10Nb-3Mo alloy, *Materials Letters*, 140 (2015) 55-58.
- [24] A. Mahboubi Soufiani, F. Karimzadeh, M.H. Enayati, Formation mechanism and characterization of nanostructured Ti6Al4V alloy prepared by mechanical alloying, *Materials & Design*, 37 (2012) 152-160.
- [25] K. Zhuravleva, M. Bönisch, S. Scudino, M. Calin, L. Schultz, J. Eckert, A. Gebert, Phase transformations in ball-milled Ti–40Nb and Ti–45Nb powders upon quenching from the β -phase region, *Powder Technology*, 253 (2014) 166-171.

- [26] Y. Long, H. Zhang, T. Wang, X. Huang, Y. Li, J. Wu, H. Chen, High-strength Ti–6Al–4V with ultrafine-grained structure fabricated by high energy ball milling and spark plasma sintering, *Materials Science and Engineering: A*, 585 (2013) 408-414.
- [27] Powder Diffraction Files: Archivos PCPDFWIN, 2.4, JCPDS-ICDD, in, 2003.
- [28] C. Suryanarayana, A. Inoue, *Bulk metallic glasses*, CRC Press, 2010.
- [29] N. Al-Aqeeli, C. Suryanarayana, M.A. Hussein, Formation of an amorphous phase and its crystallization in the immiscible Nb–Zr system by mechanical alloying, *Journal of Applied Physics*, 114 (2013) 153512-153512-153514.
- [30] A.H. Taghvaei, J. Bednarčik, J. Eckert, Influence of annealing on microstructure and magnetic properties of cobalt-based amorphous/nanocrystalline powders synthesized by mechanical alloying, *Journal of Alloys and Compounds*, 632 (2015) 296-302.
- [31] C. Aguilar, F. Castro, V. Martínez, D. Guzmán, F. de las Cuevas, L. Lozada, N. Vielma, Structural study of nanocrystalline solid solution of Cu–Mo obtained by mechanical alloying, *Materials Science and Engineering: A*, 548 (2012) 189-194.
- [32] Y.W. Gu, C.W. Goh, L.S. Goi, C.S. Lim, A.E.W. Jarfors, B.Y. Tay, M.S. Yong, Solid state synthesis of nanocrystalline and/or amorphous 50Ni–50Ti alloy, *Materials Science and Engineering: A*, 392 (2005) 222-228.
- [33] B. Huang, K.N. Ishihara, P.H. Shingu, Metastable phases of Al–Fe system by mechanical alloying, *Materials Science and Engineering: A*, 231 (1997) 72-79.
- [34] C. Suryanarayana, I. Seki, A. Inoue, A critical analysis of the glass-forming ability of alloys, *Journal of Non-Crystalline Solids*, 355 (2009) 355-360.
- [35] S. Sharma, C. Suryanarayana, Mechanical crystallization of Fe-based amorphous alloys, *Journal of Applied Physics*, 102 (2007) 083544.
- [36] N. Al-Aqeeli, C. Suryanarayana, M.A. Hussein, Formation of an amorphous phase and its crystallization in the immiscible Nb–Zr system by mechanical alloying, *Journal of Applied Physics*, 114 (2013) 153512.
- [37] A. Roine, HSC Chemistry 6.0, Chemical reaction and equilibrium software with extensive thermochemical database and flowsheet simulation, Outokumpu Research Oy Information Center, in, Pori, Finland, 2006.
- [38] H. Baker, *Introduction to alloy phase diagrams*, Materials Park, OH: ASM International, 1992. 1. 1, (1992) 2.
- [39] Y.V. Zhernovenkova, T.A. Sviridova, V.V. Tcherdyntsev, S.D. Kaloshkin, A.L. Pomadchik, Amorphous and quasicrystalline Ti–Ni–Zr powders synthesized by mechanical alloying, *Journal of Non-Crystalline Solids*, 353 (2007) 3429-3433.
- [40] G. Toop, Predicting ternary activities using binary data, *Transactions of the Metallurgical Society of AIME*, 233 (1965) 850-854.
- [41] W. Zhi-Chang, R. Lück, B. Predel, New models for computing thermodynamic properties and phase diagrams of ternary systems Part 1. Three-factor models, *Calphad*, 14 (1990) 217-234.
- [42] F. Kohler, *Monatsh. Chem*, 91 (1970) 738.
- [43] D. Manasijević, D. Živković, K. Iwao, Ž.D. Živković, Calculation of the thermodynamic properties of the Ga–Sb–Ti liquid alloys, *Journal of the Serbian Chemical Society*, 70 (2005) 9-20.
- [44] O. Redlich, A. Kister, C. Turnquist, Thermodynamics of solutions-analysis of vapor-liquid equilibria, in: *Chemical Engineering Progress Symposium Series*, Amer Inst Chemical Engineers 345 E 47TH ST, New York, NY, 1952, pp. 49-61.
- [45] M. Hoch, Application of the hoch-arpshofen model to ternary, quaternary, and larger systems, *Calphad*, 11 (1987) 219-224.
- [46] A. Miedema, P. De Chatel, F. De Boer, Cohesion in alloys—fundamentals of a semi-empirical model, *Physica B+ C*, 100 (1980) 1-28.
- [47] A. Niessen, A. Miedema, F. De Boer, R. Boom, Enthalpies of formation of liquid and solid binary alloys based on 3d metals: IV. Alloys of cobalt, *Physica B+ C*, 151 (1988) 401-432.
- [48] C. Aguilar, D. Guzmán, F. Castro, V. Martínez, F. de las Cuevas, S. Lascano, T. Muthiah, Fabrication of nanocrystalline alloys Cu–Cr–Mo super saturated solid solution by mechanical alloying, *Materials Chemistry and Physics*, 146 (2014) 493-502.
- [49] W.C. Wang, J.H. Li, H.F. Yan, B.X. Liu, A thermodynamic model proposed for calculating the standard formation enthalpies of ternary alloy systems, *Scripta Materialia*, 56 (2007) 975-978.
- [50] M. Rafiei, M.H. Enayati, F. Karimzadeh, Thermodynamic analysis of solid solution formation in the nanocrystalline Fe–Ti–Al ternary system during mechanical alloying, *The Journal of Chemical Thermodynamics*, 59 (2013) 243-249.
- [51] H. Bakker, G.F. Zhou, H. Yang, Mechanically driven disorder and phase transformations in alloys, *Progress in Materials Science*, 39 (1995) 159-241.

- [52] L. Gallego, J. Somoza, J. Alonso, Glass formation in ternary transition metal alloys, *Journal of Physics: Condensed Matter*, 2 (1990) 6245.
- [53] S. Xi, K. Zuo, X. Li, G. Ran, J. Zhou, Study on the solid solubility extension of Mo in Cu by mechanical alloying Cu with amorphous Cr(Mo), *Acta Materialia*, 56 (2008) 6050-6060.
- [54] ASM Handbook: Alloy phase diagrams, vol. 3, in: Alloy phase diagrams, ASM, Metals Park, OH, 1992.

ACCEPTED MANUSCRIPT

Thermodynamics analysis of extension of solid solution of the Ti-Nb-Ta-Mn system

Formation of amorphous phase and intermetallic compounds were observed

Nanocrystalline intermetallic compounds were formed with the sizes between 3 to 20 nm

ACCEPTED MANUSCRIPT